

Original Article

Critical Grid Power Quality Enhancement by Adaptive Hybrid Controllers Integrated PV Connected Multilevel Dual Converter Topology

B. Rupa¹, J. Namratha Manohar², M. Manjula³

^{1,3}Department of Electrical Engineering, Osmania University, Telangana, India.

²Electrical Engineering Department, Muffakham Jah College of Engineering and Technology, Telangana, India.

¹Corresponding Author : rupaboddapati05@gmail.com

Received: 08 February 2024

Revised: 08 March 2024

Accepted: 07 April 2024

Published: 30 April 2024

Abstract - In this paper, a dual converter topology is introduced to improve the power quality of the distribution system. A dual converter topology with a common link capacitor and Photo Voltaic (PV) array is connected to the low-voltage line to improve the power quality. The PV source injects active power into the line for the reduction of power consumption from conventional sources. One of the converters is connected in series, and the other is connected in parallel or shunt to the low-voltage line. The series-connected converter compensates for the voltage fluctuations and drops, whereas the shunt-connected converter mitigates the harmonics generated by the non-linear load. Both converters work in synchronization with the main source voltage by taking feedback from the source voltages. The shunt converter is operated with different control algorithms which improve the harmonic mitigation in the source side. Initially, a traditional Proportional Integral (PI) controller is introduced as a DC voltage regulator in the shunt controller. Later the PI controller is replaced with Proportional Resonant (PR) and Adaptive Fuzzy - PI (AF-PI) controller for better performance of the DC voltage regulator. With the new adaptive controllers, the damping and oscillations are reduced to a great extent reducing the harmonic content in the voltage and currents on the main source side. A comparative analysis is carried out with these mentioned controllers using MATLAB software, validating the results using tools from Simulink software. A comparison table will be provided comparing different parameters of the system and determining the best controller.

Keywords - Photo Voltaic (PV), Proportional Integral (PI), Proportional Resonant (PR), Adaptive Fuzzy - PI (AF-PI), MATLAB.

1. Introduction

With the expansion of the grid to longer and larger areas for compensating large and heavy loads, the power quality is compromised. Different types of loads connected to a single grid pollute the devices connected to it also damaging them. Apart from these polluting loads, there are other factors, such as natural phenomena like lightning, line faults due to external objects, or line disconnection due to natural disasters. Because of these faults and loads, the voltage magnitude and structure are affected, which in turn affects the currents of other equipment. These faults create voltage sags, swells, and harmonics in the grid, which are considered to be the most affecting power quality issues. To mitigate these issues several devices like Flexible AC Transmission System (FACTS) devices, Distribution Generation (DG) units, or capacitor banks are integrated into the grid [1].

The capacitor banks can compensate only the reactive power requirement of the load. This reactive power compensation only improves the voltage magnitude of the bus to which it is connected. Overcompensation at the bus (more reactive power) leads to a swell in the voltage magnitude, which may cause more adverse issues on the grid. The DG

units are renewable power generators that induce renewable power at a local bus with very little possibility of solving the power quality issues [2].

The FACTS devices are considered to be power quality improvement devices. These devices are designed with power electronic circuits operated in synchronization with the grid to which it is connected. The FACTS are different types; some are connected in series, and some in shunt to the grid. The series circuits are considered to be voltage modules, and shunt circuits are current modules.

In previous research, the series modules connected to the grid provide voltage compensation, which maintains stable voltage in the grid [3]. On the other hand, shunt modules are connected to provide harmonic and reactive power compensation to the grid. There are many publications [4] on the series modules, which can be Static Series Synchronous Compensator (SSSC), Dynamic Voltage Restorer (DVR), Series Active Power Filter (APF), etc. The shunt modules can be Static Synchronous Compensator (STATCOM), Shunt APF, VAR compensator, Thyristor Controlled Switched Reactance (TCSR), etc.



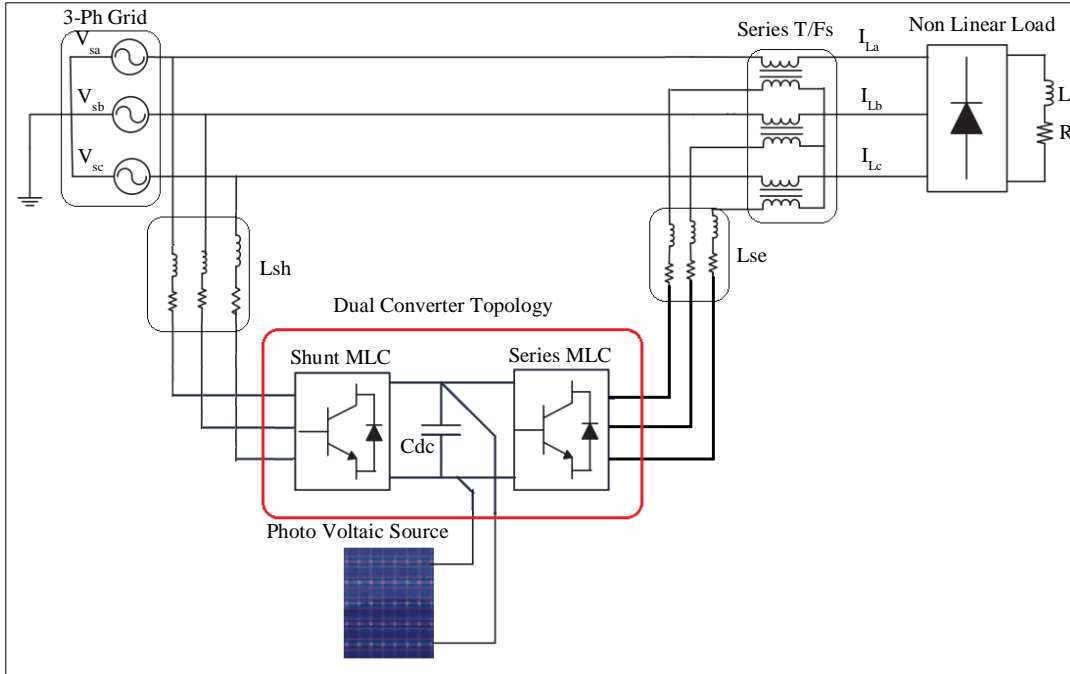


Fig. 1 MLC DCT with PV source structure

A custom device can be designed with a FACTS circuit included with renewable sources. This custom device can improve the power quality and also inject active and reactive powers into the grid [4]. As per the previous research, circuits of FACTS, back-to-back connected Voltage Source Converters (VSCs) are modelled named to be Dual Converter Topology (DCT) [5]. This DCT is connected with a common DC link capacitor on the DC sides of the VSCs. The VSCs included are 7-level cascaded H-bridge Multilevel Converters (MLC). One of the converters is connected in series and the other is connected in parallel to the grid [5]. Along with these two MLCs and capacitor elements, a PV source is also connected at the DC link for renewable power sharing.

The DCT now has the capability to improve power quality and also compensate for active and reactive powers on the grid. Figure 1 depicts the design of the MLC DCT with a PV source connected to the grid in shunt and series configuration. As observed in Figure 1 the PV source is connected at the DC link of the DCT for renewable power sharing through the MLCs. The Shunt MLC is connected at the 3-ph grid side, and the series MLC is connected at the load side through filters (Lsh and Lse).

For DC link voltage stability, a high-rating capacitor is connected at the DC link. The series converter stabilizes the voltages, and the shunt converter injects active and reactive power [6]. Both the MLC circuits are controlled by the Phase Disposition (PD) Sin Pulse Width Modulation (PWM) technique. The reference signals for the PD-PWM technique are generated by a grid Synchronization Reference Frame (SRF) controller.

The paper is arranged in Section 1, including the description of the proposed MLC PV DCT topology structure and its importance. Section 1 is followed by Section 2, which is the design of the MLC PV DCT. This section has the internal circuit modeling of the proposed topology and its operating principle. In the next Section 3 the control structure modeling for the control of cascaded MLC is designed. Advanced controllers like PR and AF-PI are introduced into the control structure, replacing traditional PI controllers for enhancement of the performance of the DCT. A comparative analysis with PI, PR and AF-PI controllers of DCT is carried out and presented in Section 4. A parametric analysis is done using a simulation of the proposed topology with the help of MATLAB Simulink tools. The final Section, 5 is the conclusion to the paper with validation of the best controller for MLC PV DCT performance followed by references.

2. MLC PV DCT Configuration

From several FACTS devices available for power quality improvement, the DCT is considered to be the most viable and optimal selection. Most of the other devices can only improve either voltage profile or current profile selectively on the source or load side. The DCT has to capability to improve both voltage and current profiles of the source and also load. The conventional DCT is a combination of two 6-switch VSC circuits connected back-to-back with a common capacitor [7]. One of the converters is connected in series on the load side and the other is connected in shunt at the source side.

For enhancement of the converter with better harmonic mitigation, the conventional 6-switch VSCs are replaced with cascaded 7-level MLCs.

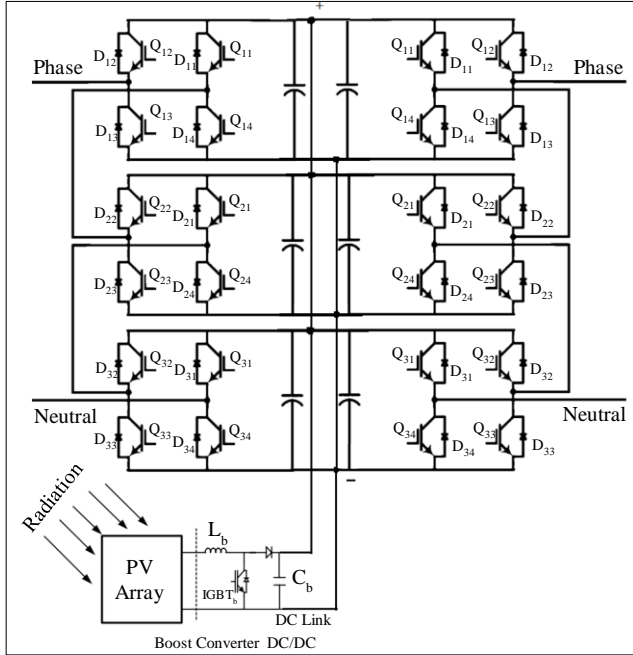


Fig. 2 7-level cascaded MLC PV DCT circuit structure for one phase

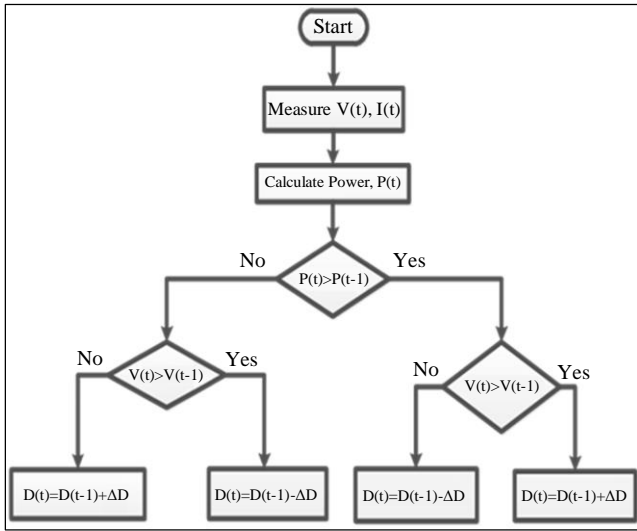


Fig. 3 P&O MPPT flow chart for duty ratio generation

Similar to the conventional DCT, the MLC DCT also has a common capacitor connected between the 7-level MLCs [8]. Along with the replacement with MLCs, a PV source is also integrated into the DCT at the DC link for renewable power sharing [9].

This renewable power is shared either through the series MLC or the shunt MLC as per the demand from the grid. A detailed internal structure of the ‘7-level cascaded MLC PV DCT’ is presented in Figure 2. The circuit in Figure 2 represents only one phase structure with 3 cascaded H-bridges connected to common DC link capacitors. All these capacitors (C_{dc1} , C_{dc2} , C_{dc3}) connected in parallel can be replaced by a

single high-rating capacitor commonly connecting the two sets of bridges [10].

All the neutral terminals from the cascaded bridges are commonly grounded, and the phases are connected to the grid in series or shunt [11]. At the common DC link, there is a PV module connected to the PV array and boost converter. The boost converter extracts maximum power from the PV array utilizing the Perturb and Observe (P&O), Maximum Power Point Tracking (MPPT) technique [12].

The converter also increases the voltage amplitude from the PV array, making the PV module share power at the specified operating voltage of the MLC DCT. The MPPT flow chart for the generation of duty ratio to the IGBT switch of the boost converter is presented in Figure 3.

As per the measured signals of the present voltage of the PV array ($V(t)$), present power of PV array ($P(t)$), past voltage of PV array ($V(t - 1)$) and past power of PV array ($P(t - 1)$) the duty ratio ($D(t)$) for the switch is calculated by the given comparative expressions:

$$D(t) = D(t - 1) + \Delta D \begin{cases} \text{If } P(t) > P(t - 1) \text{ and } V(t) > V(t - 1) \\ \text{If } P(t) < P(t - 1) \text{ and } V(t) < V(t - 1) \end{cases} \quad (1)$$

$$D(t) = D(t - 1) - \Delta D \begin{cases} \text{If } P(t) < P(t - 1) \text{ and } V(t) > V(t - 1) \\ \text{If } P(t) > P(t - 1) \text{ and } V(t) < V(t - 1) \end{cases} \quad (2)$$

Here, $D(t - 1)$ is the past value of the duty ratio, and ΔD represents the change in the duty ratio [12]. The ΔD value can be adjusted as per the response of the converter adjusting the MPPT gain (K_{mppt}) expressed as:

$$\Delta D = \int \frac{K_{mppt}}{s} Kd \quad (3)$$

Here, Kd is the percentage of duty ratio change, generally taken as ‘0.05’ (5%). Further reference signals generation for the ‘cascaded 7-level MLC DCT’ and controllers are discussed in the next section, followed by a result analysis of the design.

3. Controller Design

Both the 7-level cascaded MLC need to be controlled in synchronization with the grid voltages, as both the MLCs are connected in parallel and series connection to the grid. Both the MLCs are controlled by the PD-Sin-PWM technique, where the reference Sin signals are compared to level-shifted triangular waveforms for the generation of pulses to the switches in MLCs. The reference Sin signals are generated by SRF control designed with feedback from the grid voltages and currents [13]. Figure 4 depicts series MLC control.

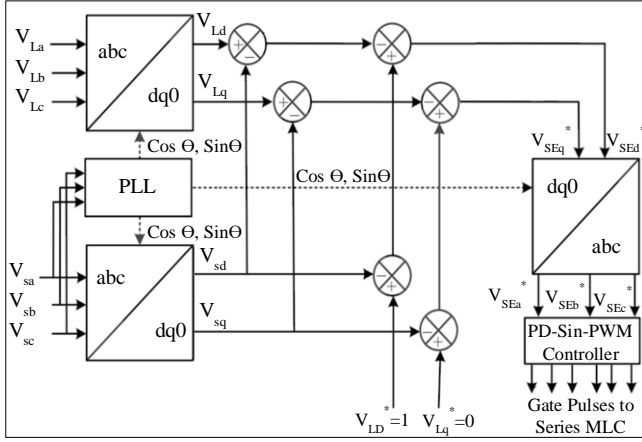


Fig. 4 Series MLC controller structure

Initially, the source and load voltages (V_{Sabc} and V_{Labc}) are transformed into dq-components for the reduction of controller complexity [14]. This is achieved by ‘Park’s transformation’ expression give:

$$\begin{bmatrix} F_d \\ F_q \\ F_0 \end{bmatrix} = \begin{bmatrix} \sin \theta & -\cos \theta & 0 \\ \cos \theta & \sin \theta & 0 \\ 0 & 0 & 1 \end{bmatrix} \begin{bmatrix} F_a \\ F_b \\ F_c \end{bmatrix} \quad (4)$$

Here, ‘ F ’ can be any variable like voltage or current. The ‘ θ ’ denotes the angle of the grid voltage of phase A determined by PLL (Phase Lock Loop). As per the generated dq-components of the source and load voltages, the reference signals (V_{SEabc}^*) for the series MLC are calculated as follows:

$$V_{SEd}^* = (V_{Ld}^* - V_{sd}) - (V_{Ld} - V_{sd}) \quad (5)$$

$$V_{SEq}^* = (V_{Lq}^* - V_{sq}) - (V_{Lq} - V_{sq}) \quad (6)$$

$$\begin{bmatrix} V_{SEa}^* \\ V_{SEb}^* \\ V_{SEc}^* \end{bmatrix} = \begin{bmatrix} \sin \theta & \cos \theta & 1 \\ \sin(\theta - \frac{2\pi}{3}) & \cos(\theta - \frac{2\pi}{3}) & 1 \\ \sin(\theta + \frac{2\pi}{3}) & \cos(\theta + \frac{2\pi}{3}) & 1 \end{bmatrix} \begin{bmatrix} V_{SEd}^* \\ V_{SEq}^* \\ V_{SE0}^* \end{bmatrix} \quad (7)$$

Here, V_{SE0}^* is taken as ‘0’, representing no biasing of signals. The given reference signals are compared to level-shifted carrier waveforms for the generation of gate pluses, as presented in Figure 5.

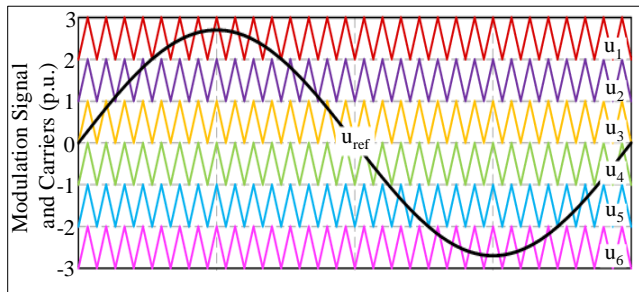


Fig. 5 PD-Sin-PWM technique

The (u_1 - u_6) signals represent carrier signals with high-frequency levels shifted, with 3 on the positive and 3 on the negative side. U_{ref} is one of the reference Sin signals generated as per equation (7). Gate pulses to each phase MLC are generated as per the U_{ref} signal [15]. Similar to the series controller, the shunt controller design is structured by replacing voltages with currents presented in Figure 6.

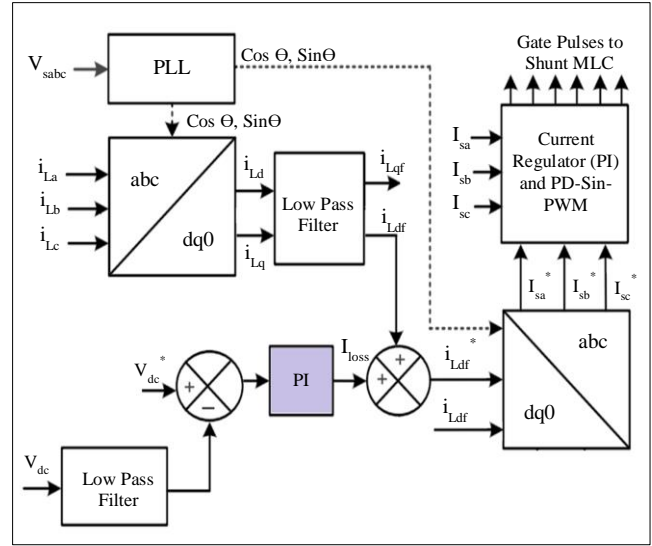


Fig. 6 Shunt MLC controller structure

The load current dq-components are generated as per expression (4) and PLL [16]. The signals i_{Ld} and i_{Lq} are filtered with a Low Pass Filter (LPF), reducing disturbances in the signals and creating filtered components i_{Ldf} and i_{Lqf} . The reference signals (i_{sabc}^*) for the converter are generated by below given expressions:

$$i_{Ld}^* = i_{Ldf} + I_{loss} \quad (8)$$

$$I_{loss} = V_{dc}^* - V_{dc} (K_{pdc} + \int K_{idc}.dt) \quad (9)$$

Here, V_{dc}^* is the reference voltage, and V_{dc} is the measured voltage of the DC link. K_{pdc} K_{idc} are the DC voltage regulator (PI controller) gains. From the reference dq-current components, the i_{sabc}^* are generated using expression (7). The i_{sabc}^* signals are compared to measured source currents (i_{sabc}), and a current regulator generates final U_{ref} signals for the shunt MLC PD-Sin-PWM technique [15].

The tuning of the voltage regulator (PI) changes the performance of the MLC. With a better adaptive and hybrid controller at the voltage regulator enhances the capability of the controller with reduced disturbances. With reduced disturbances in the controller, many factors in the system are affected, and the quality of the signals improves. Some advanced controllers are proposed in this paper which replace the conventional PI controller for performance enhancement of MLC PV DCT.

3.1. PR Controller

PI and PR controllers are considered to be similar controllers, with the PR controller having the upper hand over PI because of the integration property. The PR controller has a greater advantage of non-occurrence of static error. As the resonant frequency integrates near the fundamental frequency even phase shift does not occur.

PR controllers can be defined with specific harmonic filtration with multiple levels of creation at the R controller [17]. However, a fundamental resonant gain is connected, making the other filters optional which can be arranged as per the requirement. A simple PR controller internal structure with a harmonic compensator module is presented in Figure 7.

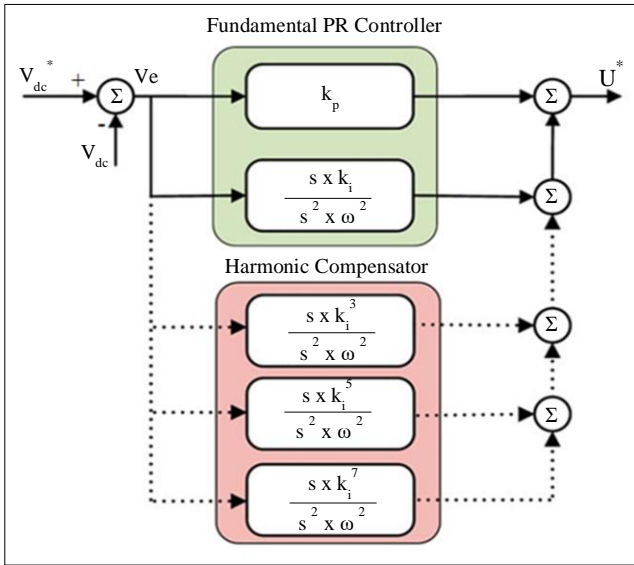


Fig. 7 PR controller internal structure

As per Figure 7 the ‘ki’ variable is considered as resonant gain tuned as per the response of the plant [18]. As per the structure, the PR controller can be expressed as:

$$u = Ve \left(k_p + k_i \left(\frac{s}{s^2 + \omega^2} \right) \right) \tag{10}$$

In the given expression (10), the variable Ve is the error voltage generated by the comparison of Vdc* and Vdc, ω is the resonant frequency. The PR controller has the ability to mitigate steady-state errors with high gain and narrow band resonant frequency. The harmonic compensator can be integrated when the controller is utilized for AC signal control.

3.2. AF-PI Controller

An AF-PI controller is an advanced hybrid controller as compared to PI and PR, as the gains (k_p k_i) are varied with respect to the error (Ve) generated [19]. The k_p k_i gains of the PI controller are selected as per the rules defined in the fuzzy design. The structure of the AF-PI controller replacing the PI voltage regulator can be observed in Figure 8.

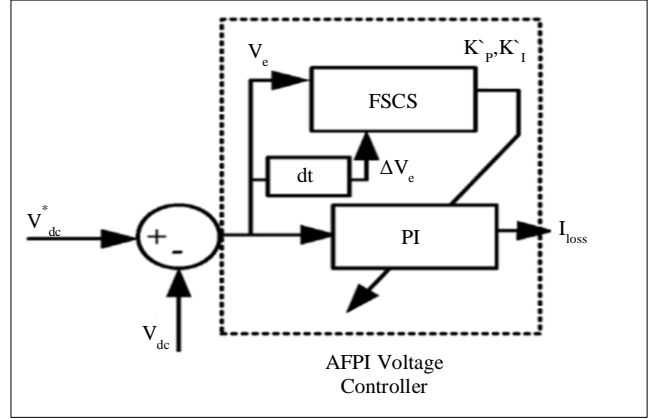


Fig. 8 AF-PI internal structure

The fuzzy design is based on ‘mamdani’ type of fuzzy with 3 variables named error (e), change in error (ce) and output (o) [20]. The output variable (o) can be either k_p or k_i gain. The variables ‘e’ and ‘ce’ are the input variables. The error variable is the ‘Ve’ generated by the DC link voltage comparison. Each input variable comprises of 5 Membership Functions (MFs) included in a triangular shape [21]. The output variable has 3 MFs with the same triangular shape. Figure 9 shows the MFs design of the input and output variables.

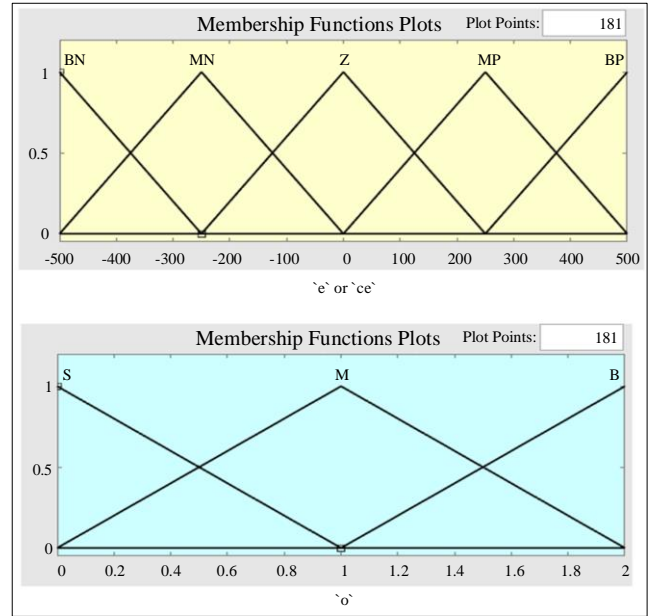


Fig. 9 MFs of variables ‘e’ or ‘ce’ and ‘o’

The input variable MFs are named Big Negative (BN), Medium Negative (MN), Zero (Z), Medium Positive (MP), and Big Positive (BP). The output variable MFs are named as Small (S), Medium (M), and Big (B). The same MFs design is maintained for the gain ‘ki’ also [22]. However, the range of the variables may vary which is set as per the response of the plant. Each gain k_p and k_i fuzzy design has its individual 25 rule base presented in Tables 1 and 2.

Table 1. 'k_p' gain rule base

25 Fuzzy Rule Base		Variable 'e'				
		BP	MP	Z	MN	BN
Variable 'ce'	BP	B	S	S	B	B
	MP	B	B	S	B	B
	Z	B	M	M	M	B
	MN	B	B	S	M	B
	BN	B	B	S	M	B

Table 2. 'k_i' gain rule base

25 Fuzzy Rule Base		Variable 'e'				
		BP	MP	Z	MN	BN
Variable 'ce'	BP	B	M	S	M	B
	MP	B	M	M	M	B
	Z	B	B	M	B	B
	MN	B	M	M	M	B
	BN	B	M	S	M	B

The fuzzy designs of k_p and k_i are updated as per the given rules, and the voltage controller of the shunt control structure is modelled. A comparative analysis is carried out with PI, PR and AF-PI controllers updated in shunt control, and the results are presented in the next section.

4. Results and Discussion

The complete design of the DCT integrated with 7-level cascaded MLI along with series and shunt controllers are modelled in Simulink of MATLAB software. The tools from the 'Powersystem' toolbox are considered for electrical circuit modeling. The controllers are modelled using 'commonly used block' sets from the Simulink library.

Table 3. Simulation parameters

Name of the Module	Parameters
Grid	3-ph 440Vrms 50Hz Infinite grid
DCT	Cascaded H-bridge 7-level module C _{dc} = 3mF, V _{dc} = 200V, R _{igbt} = 1mΩ, f _c = 5kHz
Controllers	Series controller: V _{base ph} = 240Vrms, F _o = 200Hz, V _{dref} = 1, V _{qref} = 0. Shunt Controller: F _o = 1000Hz, K _{pdc} = 2, K _{idc} = 0.005, K _{pc} = 0.017, K _{ic} = 0.00023, K _r = 10, w _c = 10, w _r = 500. 'e' range = -500 to 500, 'ce' range = -1 to 1, 'k _p ' range = 0 to 2, 'k _i ' range = 0 to 0.1. V _{dcref} = 200V.
PV Module	PV array: V _{mp} = 40.5V, I _{mp} = 6.05A, V _{oc} = 48.8V, I _{sc} = 6.43A, N _p = 5, N _s = 5, P _{pv} = 6.1kW. Boot Converter: L _b = 5mH, C _{in} = 100μF, R _{igbt} = 1mΩ.
Load	Diode Bridge rectifier Non-linear load with R = 50Ω.

The given Table 3 is the system configuration table, which includes the Simulink parameters of the model. The above parameters are considered for the model, and the simulation is run with different power quality issues set in the system.

Voltage sag swell conditions are created by the heavy load connected, and the utilization of a diode bridge rectifier generates the harmonics. Below are the graphs generated at each module when the system is operated with different operating conditions. The sags are created between 0.4-0.6sec and swells are created between 1.4-1.6sec of complete simulation time 2sec. The harmonics are injected into the source throughout the simulation by the non-linear load.

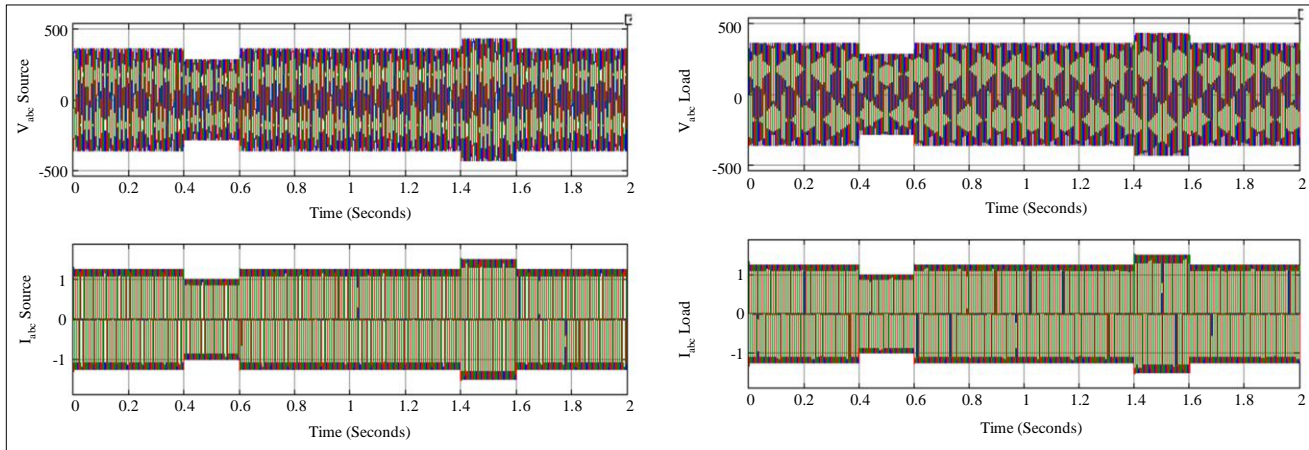


Fig. 10 3-ph voltages and currents of source and load without DCT

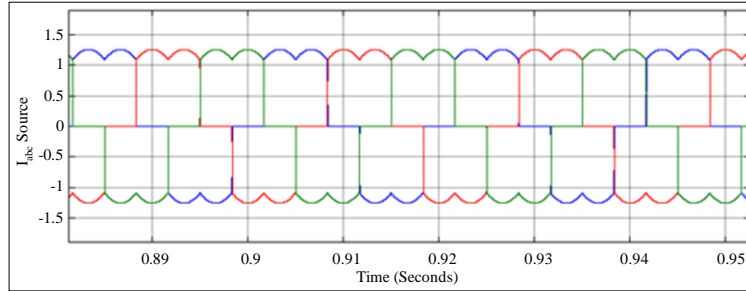


Fig. 11 3rd harmonic content of source without DCT

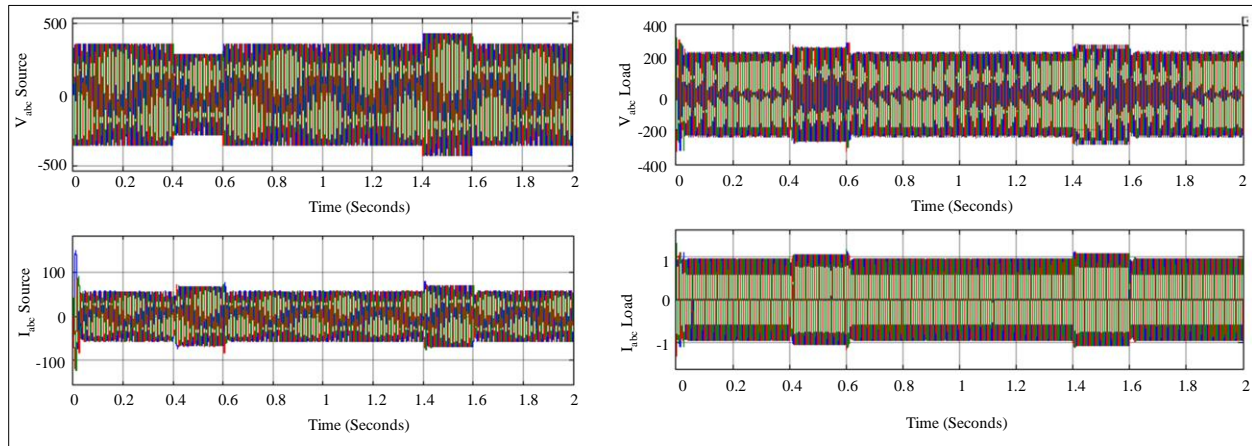


Fig. 12 3-ph voltages and currents of source and load with DCT

As per Figure 10, voltage sags, swells and current harmonics are created in both the source and load sides without DCT. The zoomed plotting of the source current graph can be observed in Figure 11 with 3rd harmonic content.

In the next simulation results the source and load voltages and currents are presented in Figure 12 with DCT connected. As observed, the sag and swells are compensated on the load side with very low voltage fluctuation.

The 3rd harmonic content in the source voltage is completely eliminated, and pure Sin waveforms can be observed in Figure 13. This is achieved by the DCT connected between the source bus and the load bus. The shunt cascaded MLC compensates for the harmonics generated by the non-linear load.

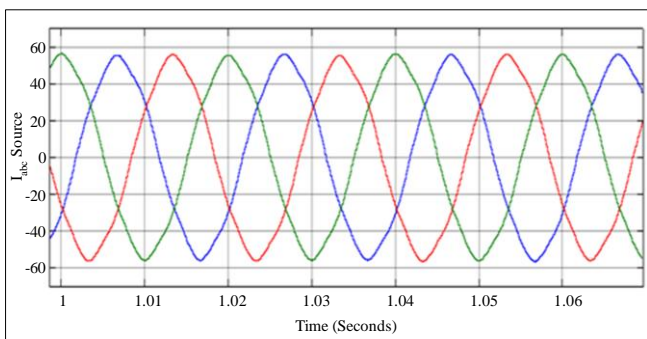


Fig. 13 Source currents with DCT

As the PV module is connected at the DC link, the PV array shares power to the grid through a boost converter operated by MPPT control. The PV array characteristics are plotted in Figure 14.

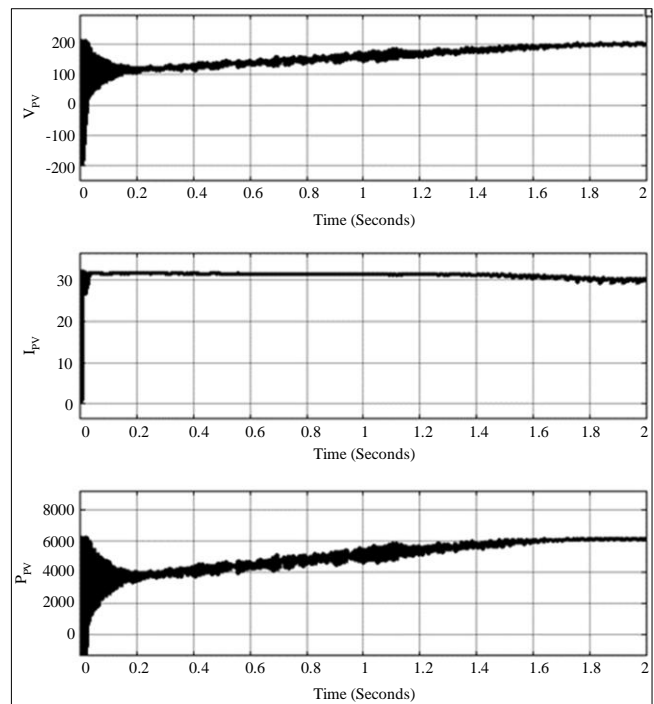


Fig. 14 PV characteristics

As per the PV characteristics, initially, the PV array injects 4kW of power, and at the end of the simulation maximum power of 6kW is extracted from the PV array. The voltage is built to 200V from the initial stage. However, the boost converter maintains the DC link voltage at 200V in Figure 15, as specified in the V_{dcref} parameter of the shunt controller. Figure 15 is a comparative graph with DC link voltage plotted for PI, PR and AF-PI voltage controllers. It is noted that the ripple in the DC link voltage is less for the AF-PI voltage controller as compared to the other two controllers (PI and PR). For the next analysis of the voltage and current graphs, the FFT analysis tool available in the ‘powergui’ block is utilized for calculating the THD of the waveforms with PI, PR and AF-PI voltage controllers.

From all the comparative graphs and THD analysis figures, a parametric comparison Table 4 is given comparing the values for the PI, PR and AF-PI controllers.

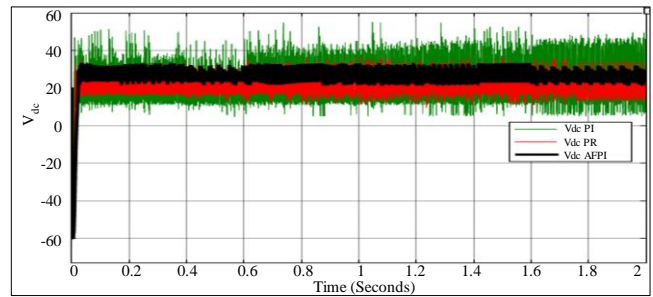


Fig. 15 DC link voltage comparison

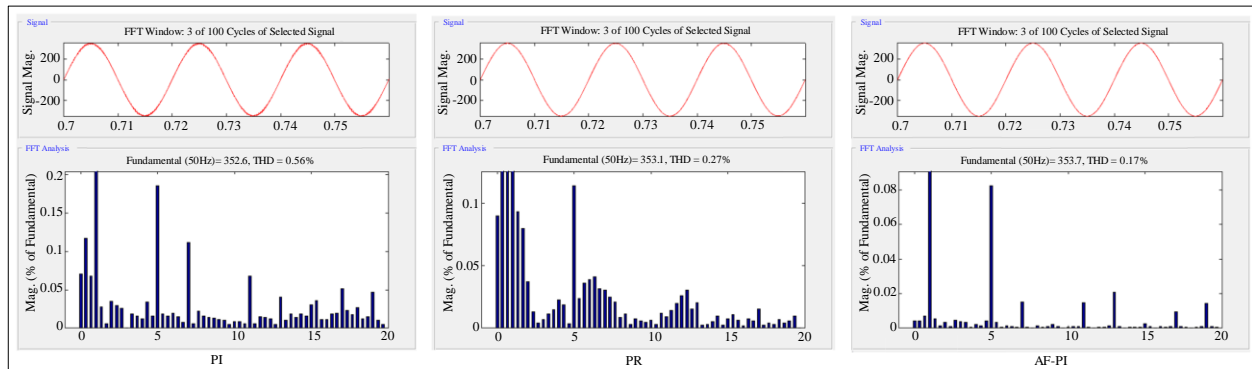


Fig. 16 THDs of source voltage with PI, PR and ANFIS

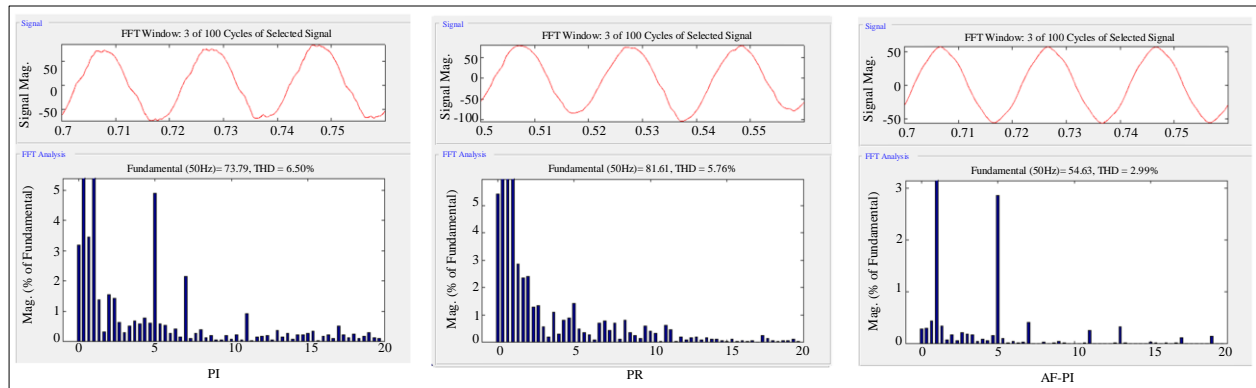


Fig. 17 THDs of source currents with PI, PR and ANFIS

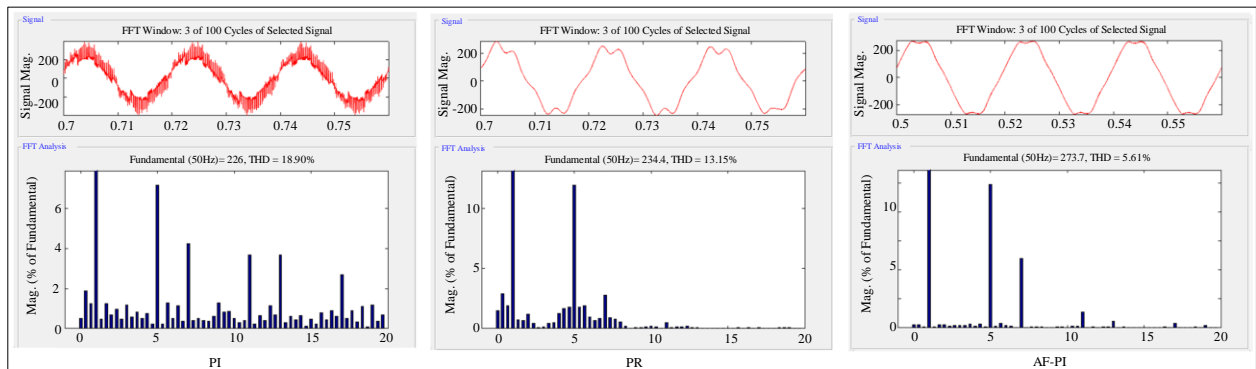


Fig. 18 THDs of load voltages with PI, PR and ANFIS

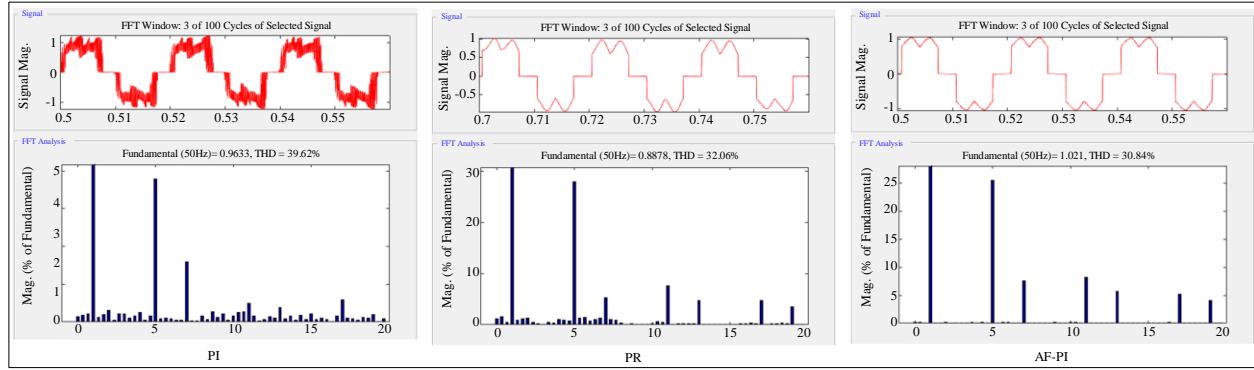


Fig. 19 THDs of load currents with PI, PR and ANFIS

Table 4. Comparison table with different controllers

Name of the Parameter	PI (%)	PR (%)	AF-PI (%)
Vdc Ripple	54.54%	28.57%	13.63%
Vsource THD	0.56%	0.27%	0.17%
Isource THD	6.5%	5.76%	2.99%
Vload THD	18.9%	13.15%	5.61%
Iload THD	39.62%	32.06%	30.84%

5. Conclusion

The performance of the DCT is enhanced by replacing the conventional 6-switch VSC modules with 7-level cascaded MLC, creating voltage levels for harmonic reduction. The design of the series and shunt controllers create stable voltages on the source and load side, along with reduced harmonics in all voltages and currents. The shunt controller configured with a traditional PI controller is replaced with advanced and hybrid PR and AF-PI controllers for better stability. These controllers are updated at the voltage regulator of the shunt controller, stabilizing the I_{loss} signal.

The error disturbance is reduced while operating the system in different operating conditions creating lower DC link voltage for AF-PI controller recorded at 13.63%. This ripple content in the DC link voltage with the AF-PI controller is far less compared to PI and PR controllers. Along with these, the THDs of the source voltages, currents, load voltage, and currents are less for PR compared to PI and less for AF-PI compared to PR. The parametric comparison table depicts that the MLC PV DCT integrated with the AF-PI controller has more stability as compared to conventional controller PI and PR.

References

- [1] Joao L. Afonso et al., "A Review on Power Electronics Technologies for Power Quality Improvement," *Energies*, vol. 14, no. 24, pp. 1-71, 2021. [[CrossRef](#)] [[Google Scholar](#)] [[Publisher Link](#)]
- [2] Tomislav Dragicevic et al., "DC Microgrids-Part II: A Review of Power Architectures, Applications, and Standardization Issues," *IEEE Transactions on Power Electronics*, vol. 31, no. 5, pp. 3528-3549, 2016. [[CrossRef](#)] [[Google Scholar](#)] [[Publisher Link](#)]
- [3] Min Soo Kim et al., "Soft Start-Up Control Strategy for Dual Active Bridge Converter with a Supercapacitor," *Energies*, vol. 13, no. 16, pp. 1-18, 2020. [[CrossRef](#)] [[Google Scholar](#)] [[Publisher Link](#)]
- [4] N. Gowtham, and Shobha Shankar, "UPQC: A Custom Power Device for Power Quality Improvement," *Materials Today: Proceedings*, vol. 5, no. 1, part 1, pp. 965-972, 2018. [[CrossRef](#)] [[Google Scholar](#)] [[Publisher Link](#)]
- [5] Serafin Ramos-Paz, Fernando Ornelas-Tellez, and J. Jesus Rico-Melgoza, "Power Quality Enhancement through Ancillary Services Provided by Power Electronic Converters," *Electric Power Systems Research*, vol. 209, 2022. [[CrossRef](#)] [[Google Scholar](#)] [[Publisher Link](#)]
- [6] Javier Riedemann Aros, Ruben Pena Guinez, and Ramon Blasco Gimenez, "Dual-Inverter Circuit Topologies for Supplying Open-Ended Loads", *Recent Developments on Power Inverters*, 2017. [[CrossRef](#)] [[Google Scholar](#)] [[Publisher Link](#)]
- [7] Michal Gwozdz, "Active Power Filter Based on a Dual Converter Topology," *Advanced Control of Electrical Drives and Power Electronic Converters, Studies in Systems, Decision and Control*, vol. 75, 2016. [[CrossRef](#)] [[Google Scholar](#)] [[Publisher Link](#)]

- [8] K.T. Maheswari, "A Comprehensive Review on Cascaded H-Bridge Multilevel Inverter for Medium Voltage High Power Applications," *Materials Today: Proceedings*, vol. 45, part 2, pp. 2666-2670, 2021. [[CrossRef](#)] [[Google Scholar](#)] [[Publisher Link](#)]
- [9] Pedro E. Melin et al., "Converter Based on Current-Source Inverter with DC Links Magnetically Coupled to Reduce the DC Inductors Value," *Energies*, vol. 15, no. 1, pp. 1-21, 2022. [[CrossRef](#)] [[Google Scholar](#)] [[Publisher Link](#)]
- [10] Hadeel S. Maarroof, Harith Al-Badrani, and Ahmad T. Younis, "Design and Simulation of Cascaded H-Bridge 5-Level Inverter for Grid Connection System Based on Multi-Carrier PWM Technique," *IOP Conference Series: Materials Science and Engineering*, 2021. [[CrossRef](#)] [[Google Scholar](#)] [[Publisher Link](#)]
- [11] P. Srujay et al., "Cascaded H-Bridge Multilevel Inverter for PV Applications," *Computer Communication, Networking and IoT*, vol. 459, 2022. [[CrossRef](#)] [[Google Scholar](#)] [[Publisher Link](#)]
- [12] Salman Salman, Xin Ai, and Zhouyang Wu, "Design of a P&O Algorithm Based MPPT Charge Controller for a Stand-Alone 200W PV System," *Protection and Control of Modern Power Systems*, vol. 3, pp. 1-8, 2018. [[CrossRef](#)] [[Google Scholar](#)] [[Publisher Link](#)]
- [13] Sachin Devassy, and Bhim Singh, "Design and Performance Analysis of Three Phase Solar PV integrated UPQC," *IEEE Transactions on Industry Applications*, vol. 54, no. 1, pp. 73-81, 2018. [[CrossRef](#)] [[Google Scholar](#)] [[Publisher Link](#)]
- [14] Rahul Kumar Agarwal, Ikhlak Hussain, and Bhim Singh, "Three-Phase Single-Stage Grid Tied Solar PV ECS Using PLL-Less Fast CTF Control Technique," *IET Power Electronics*, vol. 10, no. 2, pp. 178-188, 2017. [[CrossRef](#)] [[Google Scholar](#)] [[Publisher Link](#)]
- [15] G. Sridhar, P. Satish Kumar, and M. Sushama, "Phase Disposition PWM Technique for Eleven Level Cascaded Multilevel Inverter with Reduced Number of Carriers," *TELKOMNIKA Indonesian Journal of Electrical Engineering*, vol. 15, no. 1, pp. 49-56, 2015. [[CrossRef](#)] [[Google Scholar](#)] [[Publisher Link](#)]
- [16] Mukul Chourasia, and Aurobinda Panda, "Instantaneous DQ Method for UPQC with PI and Fuzzy Controller," *2014 6th IEEE Power India International Conference (PIICON)*, Delhi, India, pp. 1-6, 2014. [[CrossRef](#)] [[Google Scholar](#)] [[Publisher Link](#)]
- [17] Seyfettin Vadi, and Ramazan Bayindir, "Modeling, Analysis and Proportional Resonant and Proportional Integral Based Control Strategy for Single Phase Quasi-Z Source Inverters," *IEEE Access*, vol. 10, pp. 87217-87226, 2022. [[CrossRef](#)] [[Google Scholar](#)] [[Publisher Link](#)]
- [18] S. Salimin, A.F.M. Noor, and S.A. Jumaat, "Proportional Resonant Current Controller Strategy in Inverter Application," *International Journal of Power Electronics and Drive Systems (IJPEDS)*, vol. 10, no. 4, pp. 2238-2244, 2019. [[CrossRef](#)] [[Google Scholar](#)] [[Publisher Link](#)]
- [19] T. Vigneysh, and N. Kumarappan, "Grid Interconnection of Renewable Energy Sources Using Multifunctional Grid-Interactive Converters: A Fuzzy Logic Based Approach," *Electric Power Systems Research*, vol. 151, pp. 359-368, 2017. [[CrossRef](#)] [[Google Scholar](#)] [[Publisher Link](#)]
- [20] Tingting Wang et al., "An Adaptive Fuzzy PID Controller for Speed Control of Brushless Direct Current Motor," *SN Applied Sciences*, vol. 4, pp. 1-16, 2022. [[CrossRef](#)] [[Google Scholar](#)] [[Publisher Link](#)]
- [21] Vineet Kumar et al., "An Adaptive Robust Fuzzy PI Controller for Maximum Power Point Tracking of Photovoltaic System," *Optik*, vol. 259, 2022. [[CrossRef](#)] [[Google Scholar](#)] [[Publisher Link](#)]
- [22] R.S. Ravi Sankar, S.V. Jayaram Kumar, and G. Mohan Rao, "Adaptive Fuzzy PI Current Control of Grid Interact PV Inverter," *International Journal of Electrical and Computer Engineering*, vol. 8, no. 1, pp. 472-482, 2018. [[CrossRef](#)] [[Google Scholar](#)] [[Publisher Link](#)]